Am J Physiol Heart Circ Physiol
281: H939–H950, 2001.

Effects of erythrocyte aggregation and venous network geometry on red blood cell axial migration

JEFFREY J. BISHOP,[1] ALEKSANDER S. POPEL,[2]
MARCOS INTAGLIETTA,[1] AND PAUL C. JOHNSON[1]
[1]*Department of Bioengineering, University of California, San Diego, La Jolla, California 92093-0412; and* [2]*Department of Biomedical Engineering, Johns Hopkins University, Baltimore, Maryland 21205*

Received 20 November 2000; accepted in final form 28 March 2001

Bishop, Jeffrey J., Aleksander S. Popel, Marcos Intaglietta, and Paul C. Johnson. Effects of erythrocyte aggregation and venous network geometry on red blood cell axial migration. *Am J Physiol Heart Circ Physiol* 281: H939–H950, 2001.—Axial migration of red blood cells in small glass tubes can cause blood viscosity to be effectively independent of shear rate. However, this phase separation may not occur to the same degree in the venous network due to infusion of cells and aggregates at branch points. To investigate this hypothesis, we followed trajectories of fluorescently labeled red blood cells in the venular network of the rat spinotrapezius muscle at normal and reduced flow with and without red blood cell aggregation. Cells traveling near the wall of an unbranched venular segment migrated ~1% of the longitudinal path length without aggregation and migrated slightly more with aggregation. Venular segment length between branch points averaged three to five times the diameter. Cells in the main vessel were shifted centrally by up to 20% of diameter at branch points, reducing the migration rate of cells near the opposite wall to <1% even in the presence of aggregation. We conclude that formation of a cell-free marginal layer in the venular network is attenuated due to the time dependence of axial migration and the frequent branching of the network.

venous resistance; radial migration; red blood cell aggregation; in vivo fluorescence microscopy; venous network topology

SEVERAL WHOLE ORGAN STUDIES in skeletal muscle of the cat and dog have shown that venous vascular resistance increases as arterial pressure and blood flow rate decrease (11, 27, 28, 38). Recent studies performed in this laboratory have shown that these increases in venous resistance with decreasing arterial pressure and blood flow are not due to changes in vascular geometry, such as changes in venular diameter (5, 26), but instead are due largely to the effect of red blood cell aggregation on blood rheology (11). Increased venous vascular resistance at low flow rates due to red blood cell aggregation is consistent with earlier rotational viscometric data (12, 13). These data showed the apparent viscosity of normal human (aggregating) blood is up to an order of magnitude higher than that for nonaggregating human red blood cell suspensions at low shear rates. However, these data are in apparent disagreement with a number of other in vitro studies (3, 16, 36) in which human blood flowing through vertical glass tubes showed an increased tendency for red blood cell axial migration during aggregate formation at low flow rates, leading to a decreased fluid viscosity near the wall of the tube. Under conditions of steady-state flow, this decreased viscosity near the wall may be large enough to effectively cancel out an increase in resistance caused by the increased viscosity of the red blood cell central core (36).

As a possible mechanism to explain the increased resistance in vivo, we recently demonstrated that aggregation tends to blunt the velocity profile in venules as flow rate is reduced (6). That study showed the degree of blunting observed in venular velocity profiles at an arterial pressure of 40 mmHg could account for an increase in vascular resistance up to 100% compared with control arterial pressure if the blood viscosity near the vessel wall was not significantly altered at reduced flow. Because the viscosity of the blood near the wall is hematocrit dependent, we hypothesized that the degree of red blood cell axial migration in venules must be less than in the glass tube studies. However, in the glass tube studies, the length of the tube was several orders of magnitude greater than the tube diameter, providing conditions for this phenomenon to reach steady state. Studies of the morphology of the venous microcirculation in rat skeletal muscle show that the length of individual vessel orders (which may comprise several bifurcations) is 8–15 vessel diameters (19). It is our hypothesis that frequent venular junctions result in a continual infusion of red blood cells (or aggregates) into the peripheral layers of the vessel flow stream. Therefore, although a tendency may exist for individual cells to migrate away from the vessel wall, the topological structure of the vascular bed causes cells from side branches to be frequently introduced into the region closest to the wall, preventing the

Address for reprint requests and other correspondence: P. C. Johnson, Dept. of Bioengineering, University of California, San Diego, La Jolla, CA 92093-0412 (E-mail: pjohnson@bioeng.ucsd.edu).

The costs of publication of this article were defrayed in part by the payment of page charges. The article must therefore be hereby marked "*advertisement*" in accordance with 18 U.S.C. Section 1734 solely to indicate this fact.

development of a significant cell-depleted layer near the wall as occurs in vitro.

To test this hypothesis, we used an intravital microscope equipped with a charged-coupled device camera and gated image intensifier connected to a videocassette recorder to obtain multiple images of single red blood cells during transit through a venular network in the rat spinotrapezius muscle. Data were obtained at both control and reduced arterial pressures, with and without red blood cell aggregation. Aggregation, which is normally absent in the red blood cells of the rat, may be induced by infusion of Dextran 500.

We also measured the length of individual venular segments between venous branch points in this muscle to determine representative transit times between branch points. These data allow for a better estimate of the degree of axial migration in the venous vasculature.

MATERIALS AND METHODS

Animal preparation. The present analysis was performed on the database obtained in a study (6) of red blood cell velocity profiles in skeletal muscle venules; the animal preparation, experimental setup, and data acquisition are described in more detail in that report. To optimize the use of data, we designed the protocol to permit data acquisition for both studies. Our study was approved by the local Animal Subjects Committee. Briefly, 14 male Sprague-Dawley rats weighing between 250 and 400 g (327.4 ± 41.5 g) were anesthetized with an intraperitoneal injection of 50 mg/kg pentobarbital sodium (Abbott), and additional anesthetic was administered throughout the experiment as needed. The spinotrapezius muscle of the rat was prepared for intravital microscopy as described in previous studies (5, 6). The carotid artery was catheterized for blood withdrawals and pressure measurements; the jugular vein was catheterized for the administration of anesthetic, Dextran 500, FITC-dextran, or DiI-labeled red blood cells; and a trachea tube was inserted to assist breathing. All catheters were filled with a solution of heparinized saline (30 IU/ml) to prevent clotting. Animal handling and care followed the procedures outlined in the National Institutes of Health *Guide for the Care and Use of Laboratory Animals* (National Research Council, 1996). The study was approved by the local Animal Subjects Committee.

Microscope system. An intravital microscope (Ortholux II, Leitz) was equipped for both epi- and transillumination with Leitz ×25 [0.6 numerical aperture (NA)] and Olympus ×40 (0.7 NA) water immersion objectives and a Leitz UM20 (0.33 NA) condenser lens (6). This setup provided for total full-screen magnifications of the video image of ×750 (340 μm horizontal) and ×1,210 (210 μm horizontal) for the ×25 and ×40 objectives. The optical image was projected onto a video camera (CCD-72, Dage MTI) with an externally controlled, gated image intensifier (GenIISys, Dage MTI) connected to a videocassette recorder (SVO-9500MD, Sony) and viewed on a monitor (SSM-121, Sony). A 100-W mercury arc lamp (model 1149, Walker Instruments; Scottsdale, AZ) was used to illuminate the muscle preparation. A rotatable filter turret contained filters for viewing both DiI and FITC emissions under epi-illumination.

Aggregation, hematocrit, and pressure measurements. The degree of red blood cell aggregation and the hematocrit were measured during the control period as well as after infusion of Dextran 500. Triplicate measurements of the aggregation index (M) were made on a 0.35-μl blood sample with a photometric rheoscope (aggregometer, Myrenne; Roetgen, Germany) on the 10-s setting. The same blood sample was also used to measure the erythrocyte sedimentation rate (ESR) in microhematocrit tubes allowed to stand for 1 h. Arterial pressure was recorded from a carotid artery catheter attached to a pressure transducer (TNF-R, Viggo Spectramed) and a strip-chart recorder (Brush 2600, Gould).

Experimental protocol. A small quantity of red blood cells were removed from the animal and fluorescently labeled with the carbocyanine dye 1,1'-dioctadecyl-3,3,3′,3′-tetramethylindocarbocyanine perchlorate [$DiIC_{12}(3)$, absorption: 549, emission: 565, Molecular Probes] according to the method described by Unthank et al. (39), after which these labeled cells were infused into the animal to obtain an in vivo concentration of ~1%. A 1.0 g/100 ml solution of fluorescein-5-isothiocyanate dye (FITC "Isomer 1", Molecular Probes), which binds to plasma albumin, was infused into the bloodstream at a concentration of 6 mg/kg body wt to enable clear determination of the venular internal diameter under epi-illumination.

The microscope was focused on the equatorial plane of a 45- to 75-μm-diameter skeletal muscle venule selected for study based on the criteria of stable flow, a clear focus, and contrast of the image. In each venule selected for this study, a single side branch entered the main vessel. The junction of the branch and vessel was oriented with the main venule axis along the diagonal of the video screen to maximize the distance available to follow red blood cells. An image of the vessel was recorded under control conditions for 2-min periods with transillumination, excitation of the FITC dye, and excitation of DiI. To measure velocities at the flow rates of 1–14 mm/s encountered in this study, the rate of successive gate-open periods on the image intensifier was set to frequencies of 30–180 s^{-1}. This procedure produces multiple images of single red blood cells on one video frame when the frequency between gate-open periods is greater than the video framing rate of 30 s^{-1}. To obtain data at reduced shear rates, blood was removed from the rat via the carotid artery into a heparinized syringe until the arterial pressure was ~50 mmHg. Blood flow was allowed to stabilize at this reduced pressure after which a video image of the flow was again recorded under each of the illumination conditions for ~2 min. After being recorded at the reduced arterial pressure, blood was reinfused into the animal during 60–90 s.

This protocol was then repeated ~20 min after induction of red blood cell aggregation by the addition of Dextran 500 (average molecular mass 460 kDa; Sigma). A 6% solution of dextran (200 mg/kg body wt) was infused in 50 mg/kg increments during 2–3 min to achieve a plasma dextran concentration of ~0.6%. Values of the hematocrit and aggregation index (M) were determined 15 min after the dextran infusion. There was no apparent adverse reaction to the dextran infusion, such as a visible swelling of the limbs, in any of the rats used in this study.

Determination of red blood cell velocity and luminal position. Videotape recordings of the labeled plasma and labeled red blood cells were converted to digital format using a video capture board (DC30 Plus; miroVIDEO) installed in a microcomputer (300 MHz Pentium II; Micron) with Adobe Premier 4.0. Image files were transferred to compact disk (CD-Writer Plus 7200e; Hewlett-Packard) for analysis and storage.

Sample videomicrographs of a typical vessel geometry viewed under transillumination, DiI epi-illumination, and FITC epi-illumination are shown in a previous report (6). An image analysis software package (SigmaScan Pro 4.0; SPSS) was used to obtain *x*- and *y*-axis coordinate data for the individual positions of each red blood cell passing through

the field of view within a short (<15 s) time period. As explained in our previous report (6), we were able to distinguish and eliminate from consideration red blood cells traveling above or below the equatorial plane of the vessel using an objective image analysis technique. This procedure, which limits our database to data from only those cells within a narrow (~8 μm wide) region around the equatorial plane of the vessel, has been previously validated (37) in flowing blood in vivo on images of both blood platelets and fluorescent microspheres. The coordinate data for these cells were imported into a spreadsheet (EXCEL, Microsoft) where the radial and longitudinal positions relative to the venular wall were determined and recorded for each red blood cell. Data on venular wall position were obtained from the transillumination and FITC images and combined to obtain a composite diagram of venular wall position and individual cellular positions as shown in Fig. 1*A*.

Determination of red blood cell pathways and rates of axial migration. From the cell position diagram shown in Fig. 1*A*, cell flow pathways were traced by connecting the successive locations of individual cells as shown in Fig. 1*B*. The radial position of each cell (calculated as the distance normal to the vessel wall) was calculated, and the rate of axial migration was determined by fitting a regression line through the position points for each cell. Rates of axial migration were calculated as the radial movement per longitudinal distance traveled and are reported as percent grade (% grade) hereafter. Because we were interested in the behavior of the cells relative to the venular walls and wanted to minimize the effect of slight variations in venular diameter, a frame of reference was chosen so that each vessel was divided at the centerline, and the rates of axial migration of individual cells were determined relative to the nearest adjacent wall. Hence, a positive value for migration tendency corresponds to

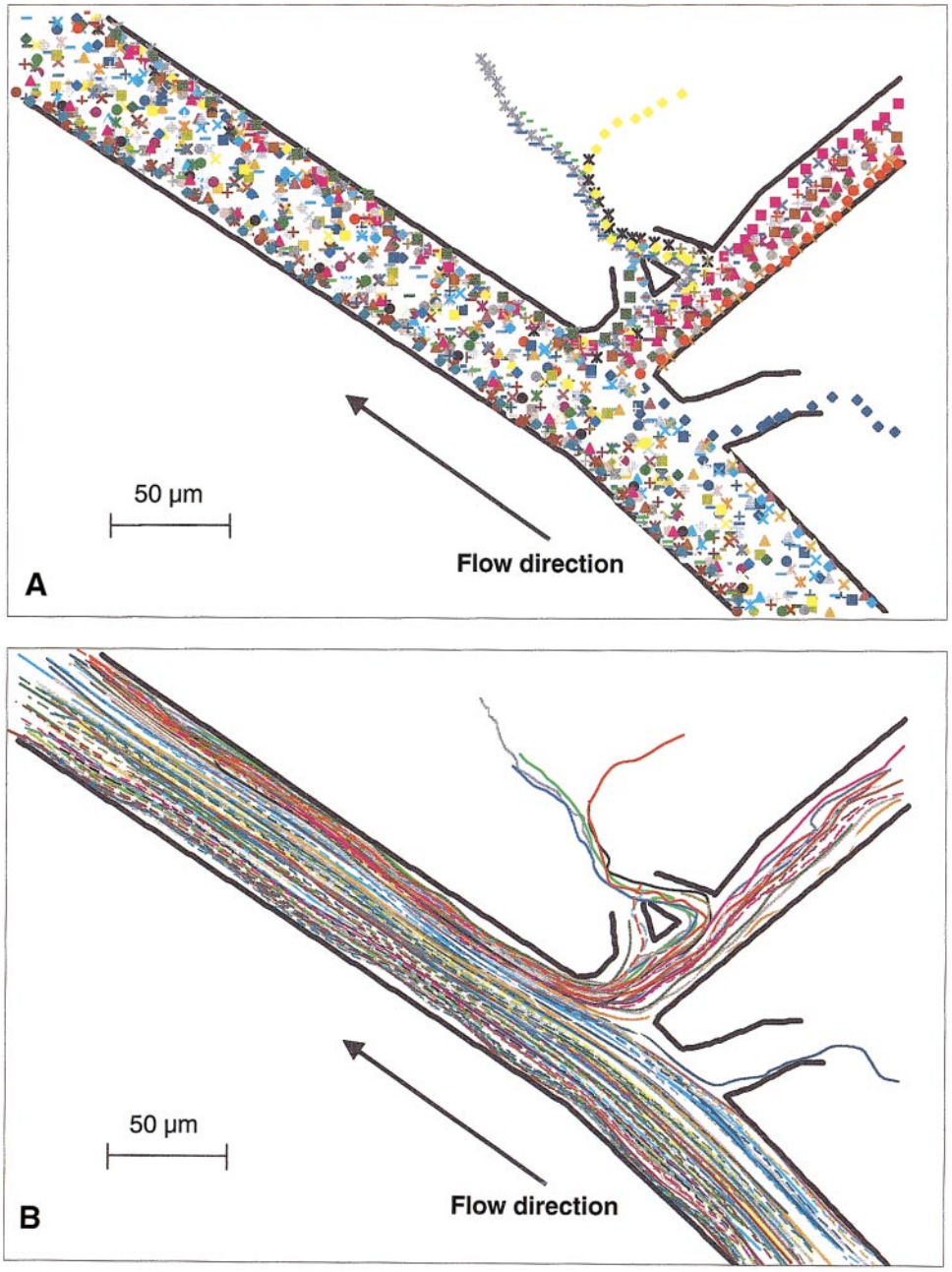

Fig. 1. Composite diagrams showing instantaneous positions (*A*) and streamlines (*B*) for normal (nonaggregating) red blood cells passing through a sample venular network at control arterial pressure. Cell positions were recorded at 5-ms intervals from DiI images, and wall position was traced from transillumination and FITC images.

a radial movement away from the vessel wall (toward the vessel centerline), and a negative value represents a radial movement toward the vessel wall. We have also determined pseudoshear rate (PSR), defined as mean red cell velocity/vessel diameter, for each condition.

Statistical analysis. Linear regression was used to determine slopes of cell pathways relative to the vessel wall. Optimal regression fits and correlation coefficients were determined using a standard software package (EXCEL, Microsoft). Differences between parameters for normal and dextran-treated rats were determined using paired *t*-tests performed by a statistical software package (SigmaStat, Jandel Scientific). Standard errors of the intercept and slope for regression lines were calculated using the standard procedures outlined by Glantz (21). For all tests and regression fits, $P < 0.05$ was considered statistically significant.

RESULTS

Hematocrit, degree of aggregation, and arterial pressure. For normal rats, the hematocrit was 45.5 ± 6.6%, the index of aggregation (M) was 0.03 ± 0.1, the ESR was 0.5 ± 0.2 mm/h, and the arterial pressures were 123 ± 11 and 50 ± 14 mmHg during control and reduced-flow protocols, respectively. In dextran-treated rats, the hematocrit was 38.9 ± 5.4%, the index of aggregation (M) was 11.7 ± 5.5, the ESR was 8.0 ± 0.4, and the arterial pressures were 132 ± 17 and 48 ± 14 mmHg for control and reduced-flow protocols, respectively. The mean hematocrit of the dextran-treated rats was significantly ($P < 0.001$) less than that of normal animals. There were no significant differences ($P > 0.05$) between arterial pressures of normal and dextran-treated animals during either the control or reduced-flow protocols.

Flow pathways of red blood cells. The positions at 33.3-ms intervals of five representative red blood cells in dextran-treated blood at reduced arterial pressure are shown in Fig. 2. As can be seen in Fig. 2, each of the cells exhibits significant fluctuations in radial position from one time point to the next. In the present study, linear regression was used to determine the tendency for axial migration during transit through the vessel. In Fig. 2, *cell A* entered from the side branch, whereas the other four cells entered from different radial positions in the main vessel. Migration rates for all cells were determined with respect to the nearest adjacent wall, so a positive slope indicates movement away from the wall toward the vessel centerline. For example, *cell E* has a slope of 0.75% after the junction and moved 0.75 μm away from the left wall during a longitudinal transit of 100 μm. From Fig. 2 it can be seen that all five cells show a tendency to migrate toward the right wall after the junction, including *cell A*, which migrated toward the right wall at a rate of 2.14% after entering the main vessel from the side branch.

Because inflow of cells from the side branch causes a large shift in radial positions and migration rates of red blood cells in the main vessel, we considered separately cell positions before, within, and beyond the planes defined by the upstream and downstream walls of the side branch (vertical dashed lines, Fig. 2). This analysis allowed us to isolate the effect of the junction from the rate of axial migration for cells in unbranched segments and to compare the magnitude of the two effects. Over 1,500 red blood cells were followed during transit through a venular junction with a side branch entering the main branch on the right side of the vessel as shown in Figs. 1 and 2.

Axial migration in unbranched segments. The rate of axial migration in an unbranched segment was determined for cells beyond the venular junction as shown in Fig. 2. These rates are plotted versus radial distance from the left wall in Fig. 3 for each of the four experimental conditions: normal (nonaggregating) blood at

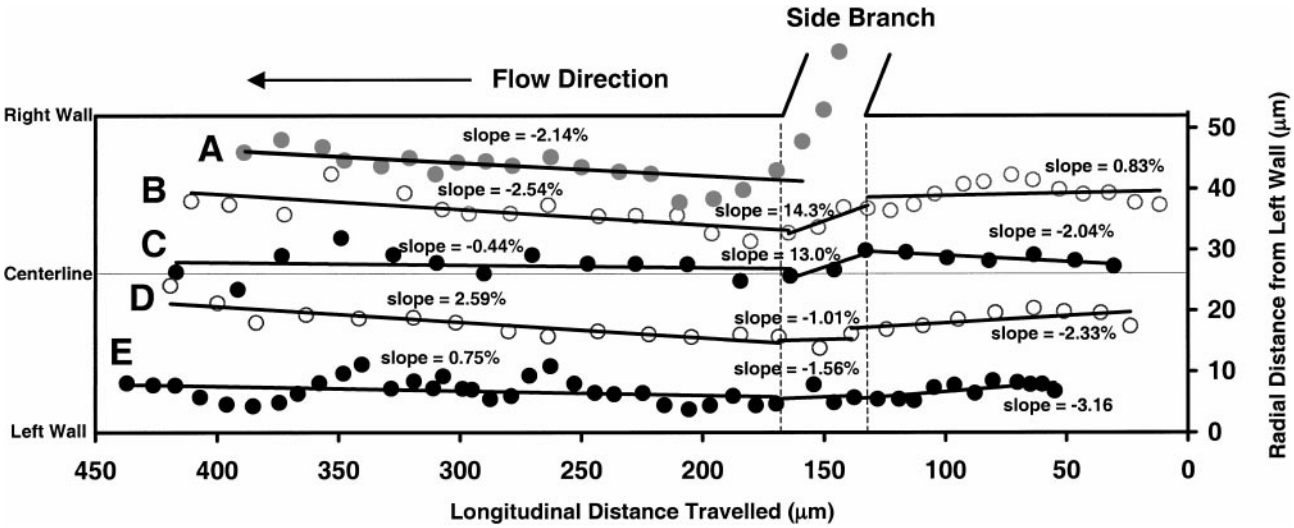

Fig. 2. Radial positions of 5 representative red blood cells (*A–E*) relative to the nearest adjacent wall of the main branch in Fig. 1. Cell positions were recorded at 33.3-ms intervals during flow of dextran-treated blood at reduced arterial pressure. Linear regression slopes shown demonstrate movements of individual cells (circles) within the main branch before, at, and after the venular junction (side branch). The radial displacement of main branch cells at the junction diminishes with radial distance from the right wall.

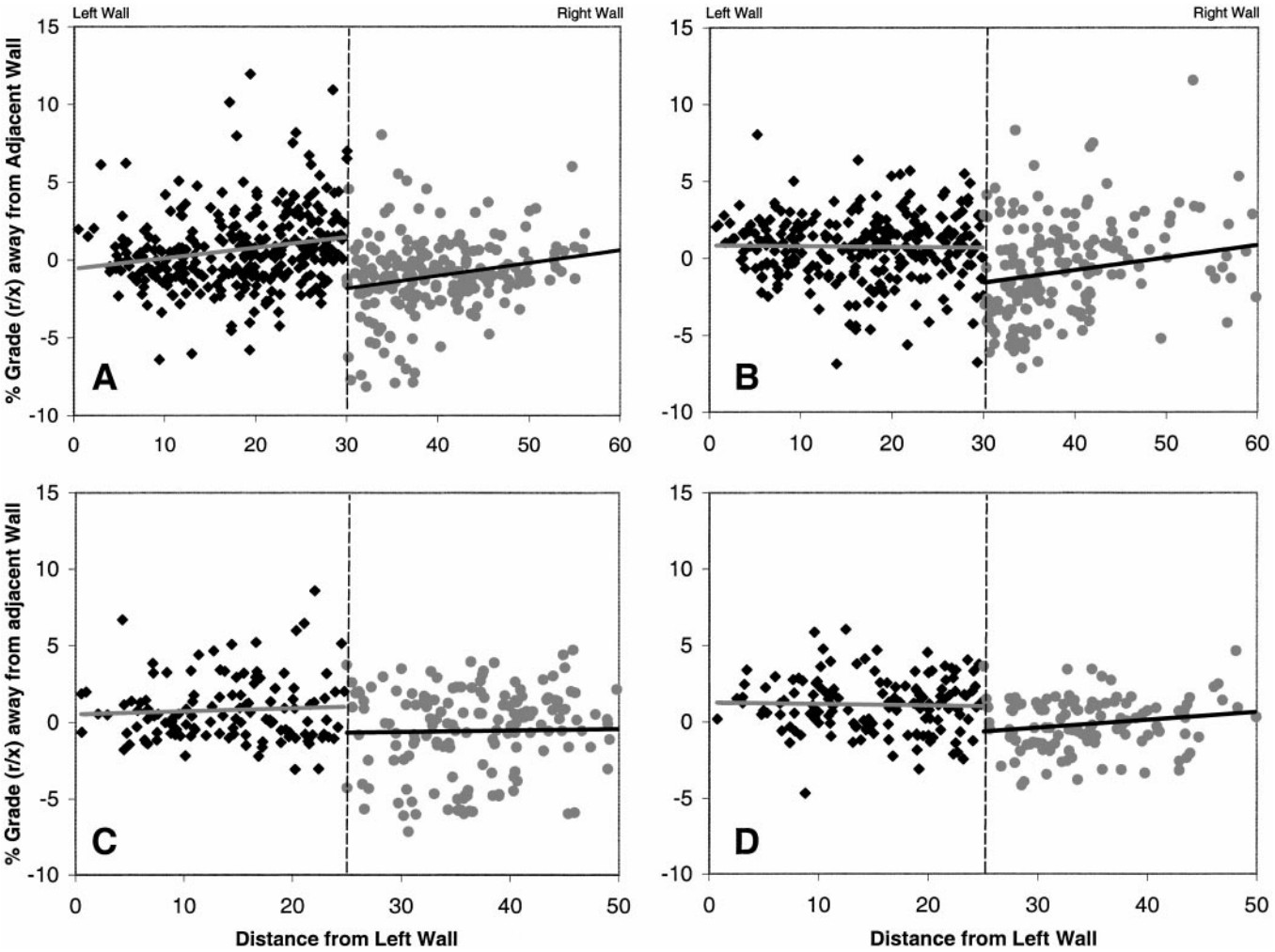

Fig. 3. Axial migration rates of red blood cells relative to the nearest adjacent wall vs. initial radial position immediately after the venous junction for each of the 4 experimental conditions of pressure and aggregation tendency. Rates are expressed as percent grade (V/x) [radial movement (μm)/ longitudinal distance traveled (100 μm)] as explained in the *Determination of red blood cell pathways and rates of axial migration*. Data are summarized below for the left wall intercept (LW intercept), right wall intercept (RW intercept), and pseudoshear rate (PSR). *A*: control pressure, normal blood; LW intercept, −0.56%; RW intercept, 0.64%; PSR, 78 ± 45 s^{-1}. *B*: control pressure, dextran-treated blood; LW intercept, 0.83%; RW intercept, 0.86%; PSR, 66 ± 26 s^{-1}. *C*: reduced pressure, normal blood; LW intercept, 0.52%; RW intercept, −0.45%; PSR, 6 ± 4 s^{-1}. *D*: reduced pressure, dextran-treated blood, LW intercept, 1.27%; RW intercept, 0.64%; PSR, 8 ± 4 s^{-1}. $P < 0.001$ for all regression lines.

control arterial pressure (*A*); dextran-treated (aggregating) blood at control arterial pressure (*B*); normal blood at reduced arterial pressure (*C*); and dextran-treated blood at reduced arterial pressure (*D*). As explained below, the vessel junction has quite a large effect on the radial distribution of cells. Although the Reynolds number ($Re = \rho D V_{mean}/\mu$, where ρ is the blood density, D is the vessel diameter, V_{mean} is the mean velocity of the blood, and μ is the blood viscosity) is <1 by approximately two orders of magnitude in these vessels, it is possible that the effects of the junction on red blood cell trajectories could extend beyond the junction. Because cells near the left wall would have been least influenced by the junction, the intercept of the regression line with the left wall (LW intercept) listed in Fig. 3 provides an estimate of the rate of axial migration for a cell traveling near the wall of an unbranched vessel segment. This rate is <1% for experimental conditions shown in Fig. 3, *A–C*, meaning that during a longitudinal transit of 100 μm, a typical cell migrates <1 μm. When dextran is present and at reduced flow rates (Fig. 3*D*), the migration rate is significantly larger (1.27%), consistent with the hypothesis that axial migration is increased by red blood cell aggregation.

The rate of axial migration for a cell near the right wall was determined from the intercept of the regression line in Fig. 3 with the right wall (RW intercept). In an undisturbed flow field, this intercept should be similar to that at the left wall, and the right and left sides of each panel would be mirror images. The values for RW intercept are of a similar magnitude (<1%) to

those for the LW intercept, but no significant difference in the slope or RW intercept can be detected in any of the four panels. This fact, combined with the differences in magnitude between the LW intercepts and the RW intercepts, illustrates the large effect of venular junctions on the distribution of cells in the network as explained below.

Flow patterns at venular junctions. It can be seen in Fig. 1 that cells from the two branches remain separated after the flow streams join. This effect can be seen more clearly in Fig. 4, where cells from the main vessel and the side branch are color coded. In fact, an overlap of <3 μm exists between the flow streams nearly 250 μm downstream from the junction. As a result, there is a radial displacement of cells entering from the main vessel as they pass the junction. Because the cells we tracked were located in the equatorial plane of the vessel, our measurements of this effect probably represent the maximal or near-maximal changes. The lateral shift of these cells as they passed the site directly opposite the upstream and downstream edges of the junction is shown in Fig. 5. The slope and intercept for dextran-treated blood at reduced arterial pressure (5*D*) are significantly ($P < 0.05$) larger than the other three conditions for reasons that are not clear, but this may reflect a larger flow contribution from the side branch. With the use of the intercept of the regression line as an estimate, those cells closest to the right wall are displaced laterally by 7–12 μm at the junction. This value, which is ~10 times larger

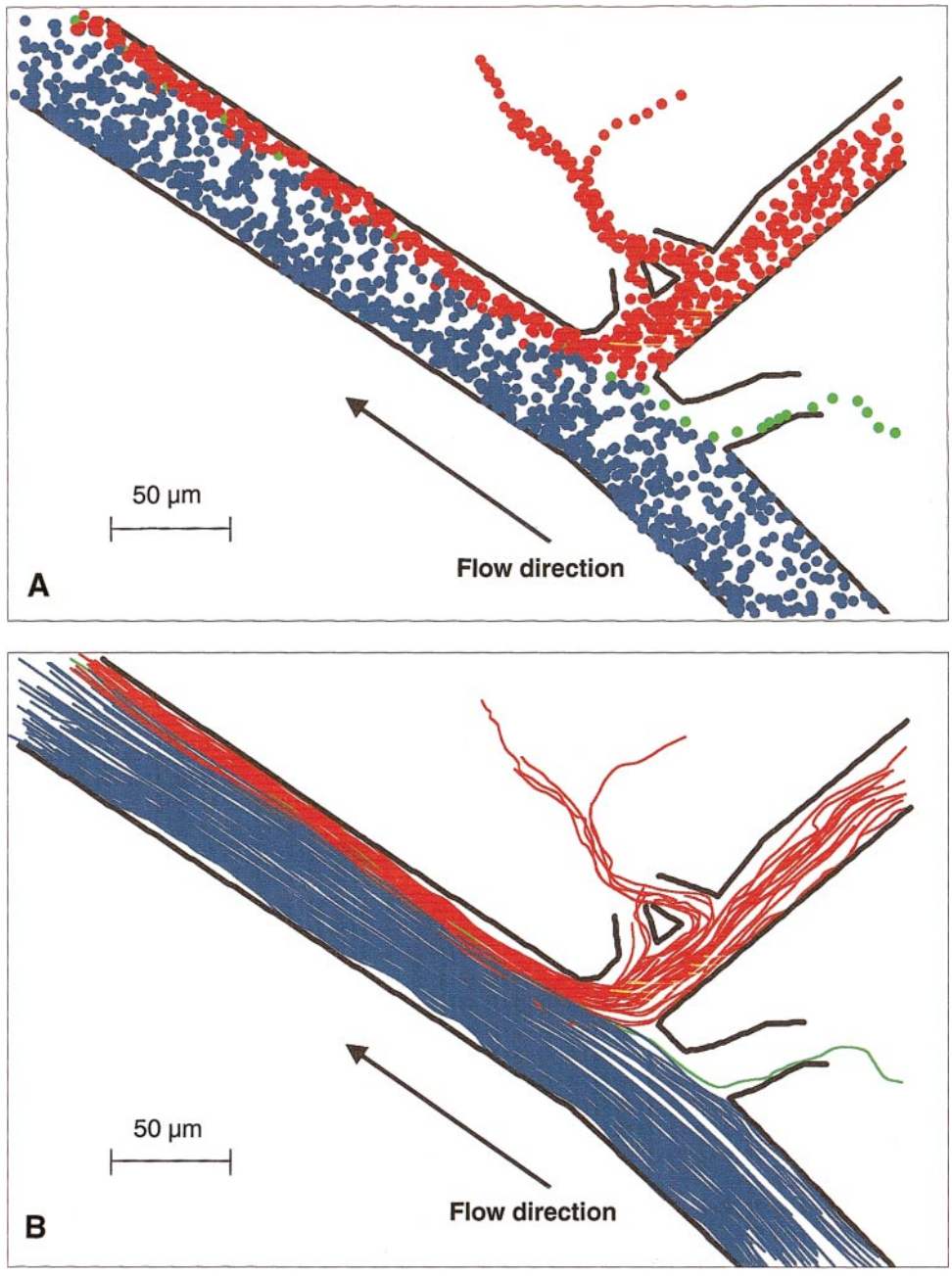

Fig. 4. Composite diagrams from data of Fig. 1 with cells' colors reflecting their branch of origin. *A*: instaneous cell positions at 5-ms intervals. *B*: trajectories of individual cells. Note the absence of mixing between flow streams from the two branches at distances as great as 200–300 μm downstream from the junction.

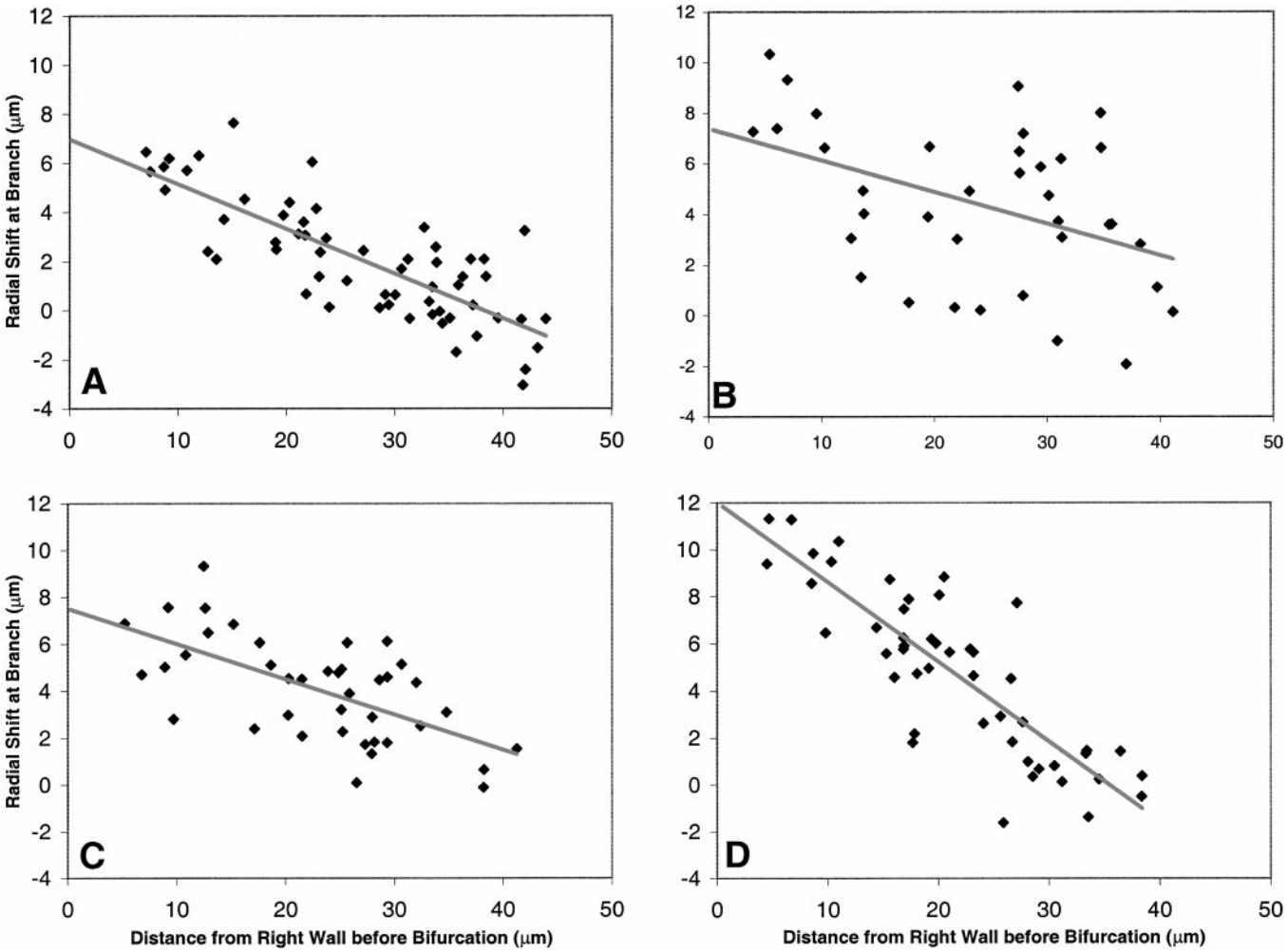

Fig. 5. Radial movement of main branch red blood cells at the branch vs. radial distance from the right wall before the branch. Distance represents the change in radial position of a red blood cell between the two planes normal to the flow direction at the walls of the entering side branch. *A*: control pressure, normal blood; slope, −0.18; intercept, 6.97 μm; PSR, 78 ± 45 s^{-1}. *B*: control pressure, dextran-treated blood; slope, −0.12; intercept, 7.37 μm; PSR, 66 ± 26 s^{-1}. *C*: reduced pressure, normal blood; slope, −0.15; intercept, 7.51 μm; PSR, 6 ± 4 s^{-1}. *D*: reduced pressure, dextran-treated blood; slope, −0.34; intercept, 12.00 μm; PSR, 8 ± 4 s^{-1}. $P < 0.01$ for all regression lines.

than the radial movements due to axial migration, emphasizes the large effect of network geometry on cell movement. The best-fit regression lines show the diminishing effect of the junction, with distance from the right wall and the value for those cells nearest to the left (distal) wall is not significantly different from zero.

Combined migration and radial shift in branching networks. The combined effect of axial migration and the radial shift at the junction determines the actual radial distribution of red blood cells within the venular network. For example, *cell B* in Fig. 2 has a migration rate of −2.54% (toward the right wall) immediately after the junction, but this movement follows a large movement toward the vessel centerline at the junction and the overall migration tendency for all of the cell positions both before and after the junction is 0.54% (away from the right wall).

This combined rate of movement over the entire length of the main vessel was determined for cells entering the field of view in the main vessel and is shown in Fig. 6 as a function of initial radial distance from the left wall for each of the four experimental conditions. Similar to that seen in the unbranched segment (Fig. 3), the migration near the left wall is <1% for each of the four experimental conditions indicating a slight tendency for cells in this location to migrate toward the center of the vessel. This tendency decreases for cells nearer the vessel centerline and is not significantly different from zero at the centerline as expected. On the right side of the vessel, the large shift of cells at the venous junction is the dominant effect, causing the RW intercept to be much larger than the LW intercept in all but Fig. 6*A*. The lack of consistency of the RW intercept and the large experimental scatter of individual cell points appears to reflect the overriding effect of the venous junction on the radial movements of red blood cells at all radial positions in the vessel.

Although those cells nearest to the left wall would be least influenced by the influx of cells from the side

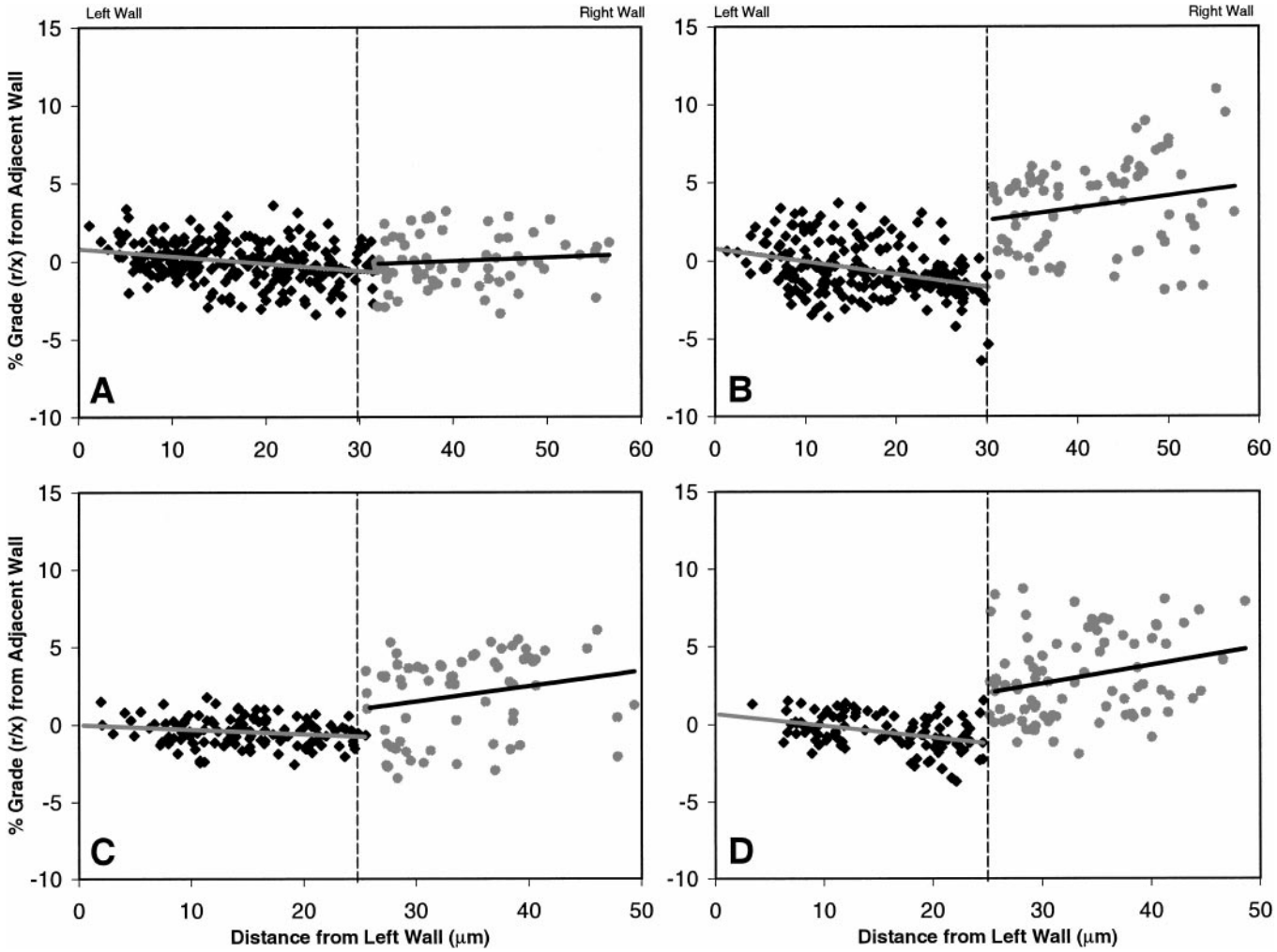

Fig. 6. Overall axial migration rates (including the effect of the venular junction) of main branch red blood cells relative to the nearest adjacent wall vs. initial radial position for each of the 4 experimental conditions of pressure and aggregation tendency. Rates are expressed as percent grade [radial movement (μm)/longitudinal distance traveled (100 μm)] as explained in the *Determination of red blood cell pathways and rates of axial migration*. *A*: control pressure, normal blood; LW intercept, −0.90%; RW intercept, 0.45%; PSR, 78 ± 45 s^{-1}. *B*: control pressure, dextran-treated blood; LW intercept, 0.75%; RW intercept, 4.93%; PSR, 66 ± 26 s^{-1}. *C*: reduced pressure, normal blood; LW intercept, −0.01%; RW intercept, 3.46%; PSR, 6 ± 4 s^{-1}. *D*: reduced pressure, dextran-treated blood, LW intercept, 0.68%; RW intercept, 4.96%; PSR, 8 ± 4 s^{-1}. $P < 0.001$ for all regression lines.

branch, a comparison of the LW intercepts from Figs. 3 and 6 reveals that the migration tendency is only slightly changed when the effect of the junction is included and the overall rate of axial migration is <1% for each of the four experimental conditions. At control arterial pressure, the value of the LW intercept for cells in dextran-treated blood (0.75%) is not significantly different from the value for cells in normal blood (0.90%). At reduced arterial pressure, the value of this intercept for cells in dextran-treated blood (0.68%) is significantly greater than the value for cells in normal blood (−0.01%). Near the right wall, the effect of the junction caused a shift of these cells as described in Fig. 5, which was 5–10 times larger than the magnitude of the migration of cells near the opposite wall.

Cellular velocities and rates of axial migration with time. Summary data on cellular velocities in this database have been reported previously (5). At control arterial pressure, the mean cellular velocities in normal and dextran-treated animals were 3.1 ± 1.7 and 2.7 ± 0.9 mm/s, corresponding to PSR rates of 78 ± 45 and 66 ± 26 s^{-1}, respectively. At reduced arterial pressure, the mean cellular velocities in normal and dextran-treated animals were 0.25 ± 0.14 and 0.31 ± 0.12 mm/s, corresponding to PSR rates of 6 ± 4 and 8 ± 4 s^{-1}, respectively. Individual cellular velocities ranged from 0.04 to 14 mm/s.

Axial migration rates per unit time for individual cells were calculated by combining the rate of axial migration per unit longitudinal distance with the velocity of the particular cell. These rates are shown in Fig. 7 for each of the four experimental conditions. The trends here for each of the experimental conditions are not different from those described above for Fig. 6.

Venular segment lengths. To determine the distance between junctions for venules of different diameters in

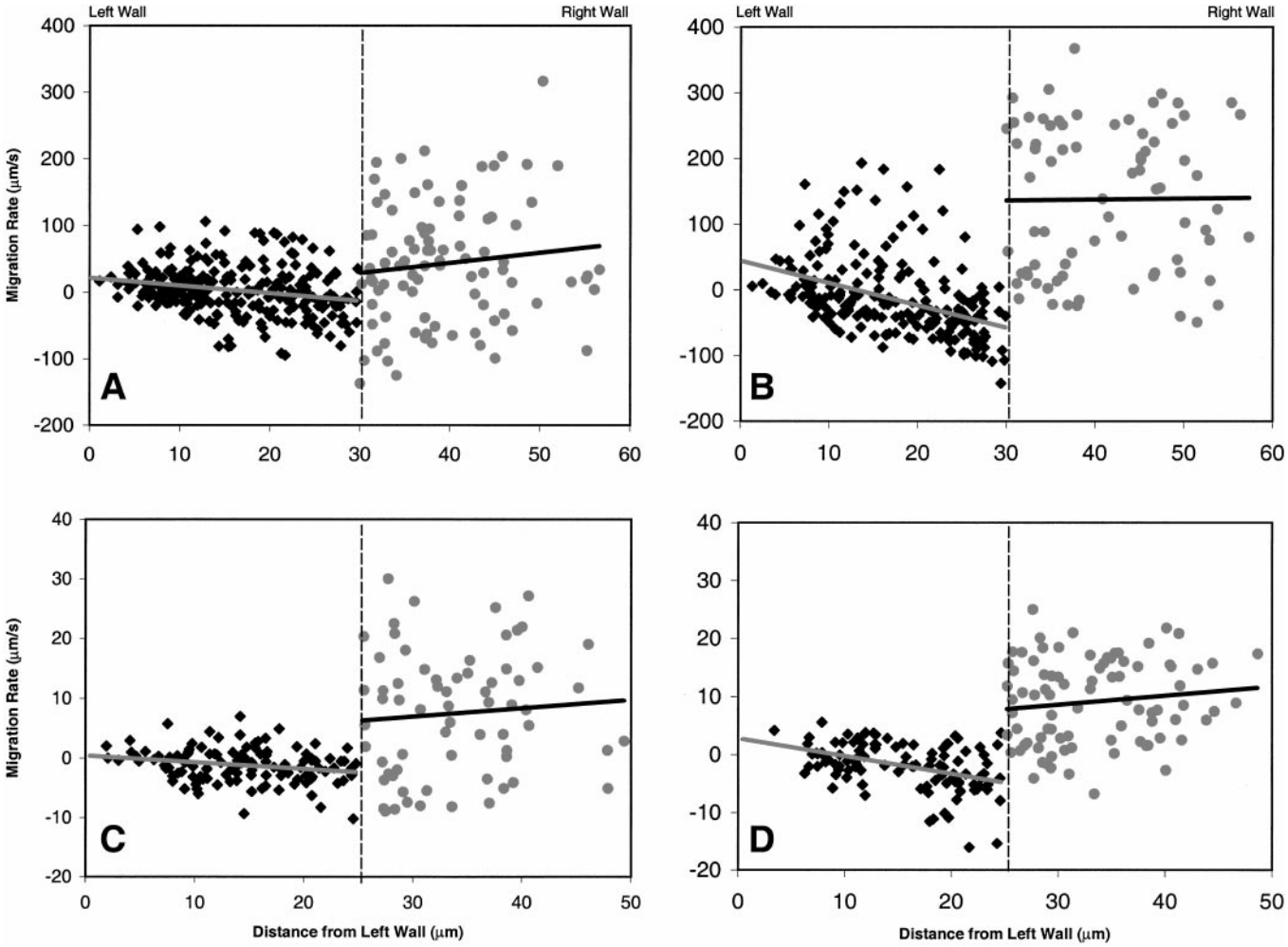

Fig. 7. Overall axial migration rates (including the effect of the venular junction) of main branch red blood cells relative to the nearest adjacent wall vs. initial radial position for each of the 4 experimental conditions of pressure and aggregation tendency. Rates are expressed in μm/s by combining data from Fig. 6 with the velocity of each red blood cell. *A*: control pressure, normal blood; LW intercept, 22 μm/s; RW intercept, 73 μm/s; PSR, 78 ± 45 s^{-1}. *B*: control pressure, dextran-treated blood; LW intercept, 44 μm/s; RW intercept, 140 μm/s; PSR, 66 ± 26 s^{-1}. *C*: reduced pressure, normal blood; LW intercept, 0.4 μm/s; RW intercept, 9.7 μm/s; PSR, 6 ± 4 s^{-1}. *D*: reduced pressure, dextran-treated blood, LW intercept, 2.8 μm/s; RW intercept, 11.7 μm/s; PSR, 8 ± 4 s^{-1}. $P < 0.001$ for all regression lines.

this muscle preparation, we measured venular diameters and lengths between branch points in four networks. For 262 venules in the diameter range of 10–95 μm (42.8 ± 20.5 μm), the average segment length is 160 ± 145 μm (range of 5–1,170 μm). Figure 8*A* shows the branching patterns typical of this muscle preparation. The length-diameter relations are plotted in Fig. 8*B*. Although there is considerable variability in venular segment length for venules of similar diameter, a significant correlation ($P < 0.001$) exists between diameter and length; the average segment length-to-diameter ratio is ~3:4. Using the regression line from Fig. 8*B*, the average segment lengths for the 53 ± 7.8-μm-internal diameter (ID) main branch and the 32.9 ± 8.3-μm-ID side branch venules of this study are 188 μm (range of 10–430 μm) and 133 μm (range of 10–350 μm), respectively.

DISCUSSION

Principal findings. We have found that axial migration rates for red blood cells near the vessel wall in unbranched 50-μm-diameter skeletal muscle venular segments of the rat were ~1 μm/100 μm longitudinal distance traveled (1%). The value was greater for dextran-treated (aggregating) blood than for nonaggregating blood (Fig. 3). Because the average length of venular segments in this tissue is ~190 μm (Fig. 8) for 50-μm-ID venules, axial migration on the order of 2–5 μm could take place between successive venular junctions. However, at venular junctions, the influx of cells from the side branch counteracts axial migration tendencies so that the rate of migration at the opposite wall is reduced to <1% under each of the experimental conditions (Fig. 6). Cells in the main channel located near the branching wall are shifted by up to 12 μm due

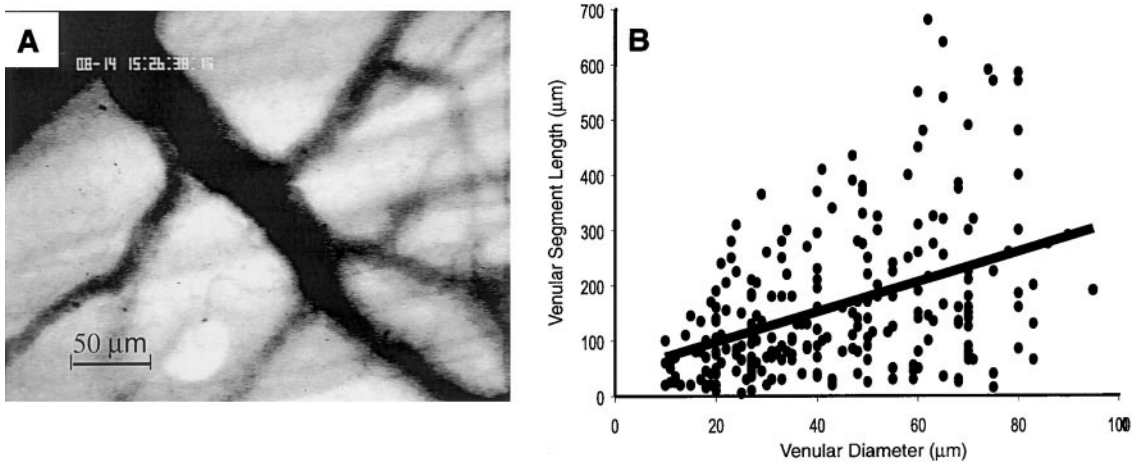

Fig. 8. *A*: sample videomicrograph of venular network of rat spinotrapezius muscle. *B*: data from 4 muscles showing the length of venular segments between venous branch points vs. venular diameter for venules of the rat spinotrapezius muscle. Linear regression line represents a significantly good fit ($r^2 = 0.1487$; $P < 0.001$) over the diameter range of 10–90 μm.

to this influx (Fig. 5). This factor, together with random collisions among red blood cells, would tend to impede axial migration and development of a cell-free layer at the vessel wall.

Limitations of measurement. The sources of error in the present study are principally associated with determination of the position of the red blood cells and the venular wall with the image analysis software. The radial component of the error as reported elsewhere (6) was 0.40 ± 0.18 μm and was independent of cellular velocity. Because these are independent random errors for each cell position, they should not significantly affect the present results due to the large number of experimental observations.

There is a concern that the large dispersions in radial position from one time point to the next could distort the slopes of regression lines drawn through such data. Because these dispersions due to random cell-cell interactions are large compared with the migration tendency, as seen in Fig. 2, a large number of observations was obtained to determine whether systematic trends and relationships exist within the data. Even considering these large dispersions, regression lines drawn through data for individual cells represented a significantly good ($P < 0.05$) fit in every case where the slope of the line was significantly different from zero to produce a meaningful correlation coefficient. In addition, the close agreement in slopes between the large number of individual cells traced produces the significant ($P < 0.05$) relationship between axial migration rate and radial position shown in Figs. 3 and 6.

Although venular diameters may vary slightly along the longitudinal axis due to lumen irregularities, we assumed a smooth inner wall with a constant venular diameter. As reported elsewhere (6), the error associated with this approximation was determined by comparison of the actual with the average wall position at 0.8-μm intervals, and the standard deviation of the difference between them was 0.74 μm. Because cell distances from the vessel wall were calculated based on this average wall position, this quantity represents the maximum error for a single cell position. However, these errors are also independent and random and should not have a significant effect on the slope of the regression line.

Venular segment lengths. In this study, the length of venular segments between junctions varied between 10 and 700 μm for venules of 10–90 μm diameter (Fig. 8*B*). The mean segment length-to-diameter ratio was ~3.5:1. A previous study of venular orders in this muscle reported venular order length-to-diameter ratios of ~10:1 (19), whereas in cat sartorius muscle ratios of between 8:1 and 30:1 for orders of venules of similar diameters to those of the present study were reported (26). However, individual orders typically contain more than one segment. For example, in rat mesenteric venules, Ley et al. (29) observed 20–30 vessel segments within four vessel orders as defined by the Horton-Strahler classification scheme. If a similar relationship exists in muscle, our findings would be consistent with previous reports of venular length-to-diameter ratios. The relationship between diameter and segment length in our study, although significant, was highly variable with an r^2 value of 0.15. Correlation coefficients of 0.25 and 0.44 were reported for diameter and order length in arterioles of the cat sartorius muscle (26).

Transit time and axial migration in a single venular segment. The relationship between venular length and diameter (Fig. 8*B*) was used with the experimentally obtained cellular velocities to calculate segment transit times for each of the experimental conditions. At control arterial pressure, the segment transit times for normal and dextran-treated blood were 0.054 and 0.059 s, respectively. At reduced arterial pressure, the segment transit times for normal and dextran-treated blood were 0.63 and 0.57 s, respectively. A number of in vitro studies (1–3, 14–16) investigating the time dependence of red blood cell aggregate formation and

axial migration using human blood flowing through long glass tubes have reported that on sudden reduction of shear rate to a low (<1 s^{-1}) value, the kinetics of aggregate formation and the onset of axial migration are on the order of several seconds. On the basis of these data, it would appear that transit times are too short at high flow rates to allow any aggregate formation in the venular network, whereas at low flow rates cells would have to traverse five or six venular segments for aggregation to occur. However, we routinely observe aggregates in the small venules at low-flow rates (unpublished observations). Axial migration, rather than aggregation per se, may be the rate-limiting step in the change in blood viscosity used as an indicator in the in vitro studies.

Combining the experimentally obtained transit times with the migration rates from Fig. 7, the average migration within a venular segment for a cell near the wall would be 1.19 and 2.60 μm for normal and dextran-treated animals at control arterial pressures, respectively, and 0.25 and 1.60 μm for normal and dextran-treated animals at reduced arterial pressures, respectively. These data show the expected result that migration tendency is greater at higher degrees of red blood cell aggregation. They also show that, on the average, a red blood cell near the vessel wall migrates less than one-fourth of a cell diameter before reaching a venous junction. At such time, new cells are introduced adjacent to the venular wall and any cell-depleted layer, which might have developed near the wall would be reduced, if not eliminated. However, the overall trend may be even less, because a large percentage of the cells entering from the side branch move toward the nearest vessel wall during some entrance length (see *cells A*, *B*, and *C*, Fig. 2) before beginning to migrate away from the wall and thereby reduce the effective venular segment length.

Development of a cell-free layer. As calculated in the preceding paragraph, a cell near the venular wall would migrate inward ~2 μm between successive venular bifurcations. However, using this same database, random changes in radial position of the red blood cell, as measured by the root mean square deviation, are of the same magnitude, 2.1 ± 1.2 μm (4). This dispersion is likely a result of intercellular interactions and would interfere with the development of a cell-free layer at the vessel wall. This effect has also been noted by Goldsmith and coworkers (24–25), who reported a pronounced movement of red blood cells to the periphery in concentrated suspensions under shear flow. Their theoretical analysis demonstrated the radial force balance between axial migration and the elastic compression of the concentrated red blood cell core. Although a visible cell-free layer was not observed in the present study under transillumination where pseudoshear rates approached 6–8 s^{-1} at reduced arterial pressure, we (7) observed the formation of a significant cell-free layer in the venules of this muscle beginning precipitously at pseudoshear rates <5 s^{-1}. Because the rate of axial migration increases with aggregation tendency at low shear rates and our observations (4) have shown that the magnitude of radial dispersion decreases with shear rate, the threshold point where the inward force due to axial migration becomes dominant appears to occur at a pseudoshear rate of ~5 s^{-1} or less.

Implications for venous vascular resistance. A number of in vitro studies have reported the formation of a cell-free or cell-depleted layer adjacent to the wall of long capillary tubes (8–10, 18, 31–33, 35) or a Couette viscometer (17) when human blood is studied at low shear rates. Because the geometry of the long glass tube and the rotational viscometer do not cause the continual introduction of cells adjacent to the wall, the conditions are more favorable for development of phase separation and apparent blood viscosity decreases under such conditions. However, if phase separation is prevented, apparent blood viscosity and shear rate are inversely related due to the formation of red blood cell aggregates (12, 13).

The small rates of axial migration, combined with the frequency of venous junctions reported here, and the previously reported dispersive effects of intercellular collisions are in agreement with previous in vivo studies (11, 27, 28, 30, 38). These studies show that, in species with aggregating blood, venous vascular resistance increases by >100% over the arterial pressure range studied here. In a previous study (5), we showed that red blood cell aggregation causes an increased blunting of the velocity profiles in spinotrapezius muscle venules as shear rate is reduced. We also calculated that venous vascular resistance could increase by as much as 100% if the hematocrit near the wall was not altered at low shear rates by red blood cell axial migration. The present results support the suggestion that due to the frequent branching of the venular network, net axial migration is not sufficient to substantially alter the radial distribution of red blood cells and red blood cell aggregates in that network. Another factor that may contribute significantly to the rise in venous resistance at low flow is the margination and adherence of leucocytes previously observed to occur in venules with red blood cell aggregation (20, 34). Adherent leukocytes can have a significant effect on venous vascular resistance (30).

The authors thank Patricia Nance, Masoud Paknejad, Caroline Flarity, Andilily Lai, and Nhat Nguyen for technical assistance. We also thank Amy Tsai for many helpful discussions.

This work was supported by National Heart, Lung, and Blood Institute Grants HL-52684, HL-64395, and HL-62354.

REFERENCES

1. **Alonso C, Pries AR, and Gaehtgens P.** Time-dependent rheological behavior of blood flow at low shear in narrow horizontal tubes. *Biorheology* 26: 229–246, 1989.
2. **Alonso C, Pries AR, and Gaehtgens P.** Time-dependent rheological behavior of blood flow at low shear in narrow vertical tubes. *Am J Physiol Heart Circ Physiol* 265: H553–H561, 1993.
3. **Alonso C, Pries AR, Kiesslich O, Lerche D, and Gaehtgens P.** Transient rheological behavior of blood in low-shear tub flow: velocity profiles and effective viscosity. *Am J Physiol Heart Circ Physiol* 268: H25–H32, 1995.

4. **Bishop JJ.** *Determinants of venous vascular resistance in skeletal muscle* (PhD Thesis). La Jolla, CA: Univ. of California, San Diego, 2000.
5. **Bishop JJ, Nance P, Popel AS, Intaglietta M, and Johnson PC.** Diameter changes in skeletal muscle venules during arterial pressure reduction. *Am J Physiol Heart Circ Physiol* 279: H47–H57, 2000.
6. **Bishop JJ, Nance P, Popel AS, Intaglietta M, and Johnson PC.** Effect of erythrocyte aggregation on velocity profiles in venules. *Am J Physiol Heart Circ Physiol* 280: H222–H236, 2001.
7. **Bishop JJ, Nance P, Popel AS, Intaglietta M, and Johnson PC.** Erythrocyte margination and sedimentation in skeletal muscle venules. *Am J Physiol Heart Circ Physiol* 281: H951–H958, 2001.
8. **Braasch D.** Dependence of capillary flow resistance upon the width of the marginal layer and the viscosity of the axial core. *Biorheology, Suppl* I: 135–143, 1984.
9. **Braasch D and Witte B.** Correlation between shear dependent blood viscosity, electrical resistance and calculated width of the marginal layer in blood perfused capillary tubes. *Int J Microcirc Clin Exp* 5: 347–357, 1987.
10. **Bugliarello G and Hayden JW.** Detailed characteristics of the flow of blood in vitro. *Trans Soc Rheol* 7: 209–230, 1963.
11. **Cabel M, Meiselman HJ, Popel AS, and Johnson PC.** Contribution of red blood cell aggregation to venous vascular resistance in skeletal muscle. *Am J Physiol Heart Circ Physiol* 272: H1020–H1032, 1997.
12. **Chien S.** Shear dependence of effective cell volume as a determinant of blood viscosity. *Science* 168: 977–978, 1970.
13. **Chien S, Usami S, Dellenback RJ, and Gregersen MI.** Shear-dependent interaction of plasma proteins with erythrocytes in blood rheology. *Am J Physiol* 219: 143–153, 1970.
14. **Cokelet GR.** Rheology and hemodynamics. *Annu Rev Physiol* 42: 311–324, 1980.
15. **Cokelet GR.** The rheology and tube flow of blood. In: *Handbook of Bioengineering*, edited by Skalak R and Chien S. San Francisco, CA: McGraw-Hill, 1987.
16. **Cokelet GR and Goldsmith HL.** Decreased hydrodynamic resistance in the two-phase flow of blood through small vertical tubes at low flow rates. *Circ Res* 68: 1–17, 1991.
17. **Cokelet GR, Merrill EW, Gilliland ER, and Shin H.** The rheology of human blood–measurement near and at zero shear rate. *Transfusion* 7: 303–317, 1963.
18. **Devendran T, Brandhuber M, and Schmid-Schönbein H.** Axial migration of RBC and the influence of cell flexibility and aggregation. *Bibl Anat* 13: 95–96, 1975.
19. **Engelson ET, Schmid-Schonbein GW, and Zweifach BW.** The microvasculature in skeletal muscle. Part III. Venous network anatomy in normotensive and spontaneously hypertensive rats. *Int J Microcirc Clin Exp* 4: 229–248, 1985.
20. **Fahraeus R.** The influence of the rouleau formation of the erythrocytes on the rheology of the blood. *Acta Med Scand* 161: 151–165, 1958.
21. **Glantz SA.** *Primer of Biostatistics*. San Francisco, CA: McGraw-Hill, 1997.
22. **Goldsmith HL.** Microscopic flow properties of red cells. *Fed Proc* 26: 1813–1820, 1967.
23. **Goldsmith HL.** Red cell motions and wall interactions in tube flow. *Fed Proc* 30: 1578–1588, 1971.
24. **Goldsmith HL and Marlow JC.** Flow behavior of erythrocytes. Part II. Particle motions in concentrated suspensions of ghost cells. *J Colloid Interface Sci* 71: 383–407, 1979.
25. **Goldsmith HL and Mason SG.** Axial migration of particles in Poiseuille flow. *Nature* 190: 1095–1096, 1961.
26. **House SD and Johnson PC.** Diameter and blood flow of skeletal muscle venules during local flow regulation. *Am J Physiol Heart Circ Physiol* 250: H828–H837, 1986.
27. **House SD and Johnson PC.** Microvascular pressure in venules of skeletal muscle during arterial pressure reduction. *Am J Physiol Heart Circ Physiol* 250: H838–H845, 1986.
28. **Johnson PC and Hanson KM.** Effect of arterial pressure on arterial and venous resistance of intestine. *J Appl Physiol* 17: 503–508, 1962.
29. **Ley K, Pries AR, and Gaehtgens P.** Topological structure of rat mesenteric microvessel networks. *Microvasc Res* 32: 315–332, 1986.
30. **Lipowsky HH, Usami S, and Chien S.** In vivo measurements of "apparent viscosity" and microvessel hematocrit in the mesentery of the cat. *Microvasc Res* 19: 297–319, 1980.
31. **Palmer AA.** Axial drift of cells and partial plasma skimming in blood flowing through glass slits. *Am J Physiol* 209: 1115–1122, 1965.
32. **Palmer AA.** Influence of absolute flow rate and rouleau formation on plasma skimming in vitro. *Am J Physiol* 217: 1339–1345, 1969.
33. **Palmer AA and Jedrzejczyk HJ.** The influence of rouleaux on the resistance to flow through capillary channels at various shear rates. *Biorheology* 12: 265–270, 1975.
34. **Pearson MJ and Lipowsky HH.** Influence of erythrocyte aggregation on leukocyte margination in postcapillary venules of rat mesentery. *Am J Physiol Heart Circ Physiol* 279: H1460–H1471, 2000.
35. **Reinke W, Gaehtgens P, and Johnson PC.** Blood viscosity in small tubes: effect of shear rate, aggregation, and sedimentation. *Am J Physiol Heart Circ Physiol* 253: H540–H547, 1987.
36. **Reinke W, Johnson PC, and Gaehtgens P.** Effect of shear rate variation on apparent viscosity of human blood in tubes of 29 to 94 μm diameter. *Circ Res* 59: 124–132, 1986.
37. **Tangelder GJ, Slaaf DW, Teirlinck HC, Alewijnse R, and Reneman RS.** Localization within a thin optical section of fluorescent blood platelets flowing in a microvessel. *Microvasc Res* 23: 214–230, 1982.
38. **Thulesius O and Johnson PC.** Pre- and postcapillary resistance in skeletal muscle. *Am J Physiol* 210: 869–872, 1966.
39. **Unthank JL, Lash JM, Nixon JC, Snider RA, and Bohlen HG.** Evaluation of carbocyanine-labeled erythrocytes for microvascular measurements. *Microvasc Res* 45: 193–210, 1993.